

# Pulsation in the atmosphere of the roAp star HD 24712

## I. Spectroscopic observations and radial velocity measurements<sup>\*,\*\*</sup>

T. Ryabchikova<sup>1,2</sup>, M. Sachkov<sup>2</sup>, W. W. Weiss<sup>1</sup>, T. Kallinger<sup>1</sup>, O. Kochukhov<sup>3</sup>, S. Bagnulo<sup>4</sup>, I. Ilyin<sup>5</sup>,  
J. D. Landstreet<sup>6</sup>, F. Leone<sup>7</sup>, G. Lo Curto<sup>3</sup>, T. Lüftinger<sup>1</sup>, D. Lyashko<sup>8</sup>, and A. Magazzù<sup>9</sup>

<sup>1</sup> Institut für Astronomie, Universität Wien, Türkenschanzstrasse 17, 1180 Wien, Austria

<sup>2</sup> Institute of Astronomy, Russian Academy of Sciences, Pyatnitskaya 48, 119017 Moscow, Russia  
e-mail: ryabchik@inasan.ru

<sup>3</sup> Department of Astronomy and Space Physics, Uppsala University Box 515, 751 20 Uppsala, Sweden

<sup>4</sup> European Southern Observatory, Casilla 19001, Santiago 19, Chile

<sup>5</sup> Astrophysikalisches Institut Potsdam, An der Sternwarte 16, 14482 Potsdam, Germany

<sup>6</sup> Department of Physics and Astronomy, University of Western Ontario, London, Ontario N6A 3K7, Canada

<sup>7</sup> Dipartimento di Fisica ed Astronomia, Università di Catania, via S. Sofia 78, 95123 Catania, Italy

<sup>8</sup> Taurian National University, Simferopol, Ukraine

<sup>9</sup> INAF – Telescopio Nazionale Galileo, PO Box 565, 38700 Santa Cruz de La Palma, Spain

Received 8 September 2006 / Accepted 8 November 2006

### ABSTRACT

**Aims.** We have investigated the structure of the pulsating atmosphere of one of the best studied rapidly oscillating Ap stars, HD 24712.

**Methods.** For this purpose we analyzed spectra collected during 2001–2004. An extensive data set was obtained in 2004 simultaneously with the photometry of the Canadian MOST mini-satellite. This allows us to connect directly atmospheric dynamics observed as radial velocity variations with light variations seen in photometry.

**Results.** We directly derived for the first time and for different chemical elements, respectively ions, phase shifts between photometric and radial velocity pulsation maxima indicating, as we suggest, different line formation depths in the atmosphere. This allowed us to estimate for the first time the propagation velocity of a pulsation wave in the outer stellar atmosphere of a roAp star to be slightly lower than the sound speed. We confirm large pulsation amplitudes ( $150\text{--}400\text{ m s}^{-1}$ ) for REE lines and the  $H\alpha$  core, while spectral lines of the other elements (Mg, Si, Ca, and Fe-peak elements) have nearly constant velocities. We did not find different pulsation amplitudes and phases for the lines of rare-earth elements before and after the Balmer jump, which supports the hypothesis of REE concentration in the upper atmosphere above the hydrogen line-forming layers. We also discuss radial velocity amplitudes and phases measured for individual spectral lines as tools for a 3D tomography of the atmosphere of HD 24712.

**Key words.** stars: atmospheres – stars: chemically peculiar – stars: individual: HD 24712 – stars: magnetic fields – stars: oscillations

## 1. Introduction

About 10% to 20% of upper main sequence stars are characterized by remarkably rich line spectra, often containing numerous unidentified features. Compared to the solar case, overabundances of up to a few dex are often inferred for some iron peak and rare earth elements, whereas some other chemical elements are found to be underabundant (Ryabchikova et al. 2004). Some of these *Chemically Peculiar* (CP) stars also exhibit organized magnetic fields with a typical strength of a few kG. The specific chemical peculiarities observed are believed to result from the influence of the magnetic field on the diffusing ions, possibly in

combination with the influence of a weak, magnetically directed wind (e.g., Babel 1992).

More than 30 cool CP stars exhibit an additional peculiarity, which is high-overtone, low-degree, non-radial  $p$ -mode pulsation with periods in the range of 6–21 min, with their observed pulsation amplitudes modulated according to the visible magnetic field structure. These so-called rapidly oscillating peculiar A to F-type (roAp) stars are key objects for asteroseismology, which presently is the most powerful tool for testing theories of stellar structure and evolution. Spectroscopic and photometric techniques provide information on the boundary zone relevant for any pulsation model, and open access to different modes and hence atmospheric layers. An observed phase lag between luminosity and radial velocity variations is an important parameter for a first step towards modeling the stellar structure. The dependency of radial velocity amplitudes as a function of optical depths lead to a 3D tomography of the stellar atmosphere.

The best studied multi-periodic roAp star presently is HD 24712, which makes this star a cornerstone for stellar seismology, even beyond the class of CP stars. It was discovered to be a pulsator by Kurtz (1982) with periods around 6 min, and Matthews et al. (1988) found synchronized radial velocity

\* Based on observations collected at the Canada-France-Hawaii Telescope (CFHT), at the Nordic Optical Telescope (NOT), at the European Southern Observatory, Paranal, Chile, (DDT-274.D-5011), at the Telescopio Nazionale Galileo (TNG), and from MOST, a Canadian Space Agency mission operated jointly by Dynacon, Inc., the University of Toronto Institute of Aerospace Studies, and the University of British Columbia, with assistance from the University of Vienna.

\*\* Tables 4, 5 and Fig. 9 are only available in electronic form at <http://www.aanda.org>

variations. Photometry with the Whole Earth Telescope (WET, Kurtz et al. 2002) revealed a “missing” mode, suggesting that  $p$ -mode pulsation are strongly affected by the global stellar magnetic field, an aspect which was investigated in detail by Cunha et al. (2003) and by Cunha (2006).

These characteristics made HD 24712 a very strong candidate for contemporaneous spectroscopic observations with large ground based equipment suited to obtain high time resolution, high spectral resolution, and high signal-to-noise ratio spectra simultaneously with high precision photometric observations with MOST, the Canadian photometric space telescope (Walker et al. 2003). The MOST instrument is a 15-cm Maksutov type optical telescope feeding twin CCD detectors through a broadband filter (350–700 nm). The equipment was designed to obtain rapid photometry of bright stars for up to 2 months and with a nearly 100% duty cycle. Despite its low mass of only 54 kg (and hence little inertia) it is able to perform optical photometry of point sources due to a pointing accuracy of better than  $\pm 1''$  rms (Walker et al. 2003).

MOST observed HD 24712 continuously from Nov. 5, to Dec. 4, 2004, and a parallel ground based observing campaign was organized which yielded the spectroscopic time series listed in the last five lines of Table 1. While the main photometric results will be published elsewhere, we focus here on the spectroscopic analysis and are using MOST data primarily for a direct comparison of the data taken simultaneously in space and from ground.

## 2. Observations and spectra reduction

The observations of HD 24712 were collected during 13 nights: Oct. 2–4, 2001; Sep. 23–26, 2002; Nov. 6, 2003; Nov. 11–13, 15, and Dec. 2, 2004. The journal of observations is given in Table 1, which lists set numbers, civil dates, heliocentric Julian dates of the start of the observing sequence, spectral range, run duration in hours, and the number of spectra that were obtained in each night. The chosen exposure times are a compromise between the requirement to integrate the spectrum only over a small fraction of the pulsation period, and the need to have a reasonable signal-to-noise ( $S/N$ ) ratio for each spectrum. The seventh column gives the rotation phases for the mean time of each data set according to the ephemeris given by Ryabchikova et al. (2005b):

$$\text{HJD}(\langle B_z \rangle_{\max}) = 2\,453\,235.18(40) + 12.45877(16)\,d.$$

Heliocentric Julian dates are given for the centre of exposures. The heliocentric corrections were applied to spectroscopic observations and to MOST photometry in the same way.

### 2.1. Time-series of single-order spectra

- **GECKO**: the observations of 2001 and 2002 were obtained with the single-order  $f/4$  GECKO Coudé spectrograph and the EEV1-CCD at the 3.6-m Canada-France-Hawaii telescope. The spectra have a resolving power of about 115 000, determined from the widths of a number of ThAr comparison lines. The exposure time was 60 s, dead time was 44 s, and the achieved  $S/N$  in the continuum was about 100. These observations covered 7 spectral regions centered approximately at 4860, 5300, 5855, 6160, 6600, 6675, and 7780 Å, containing the most interesting spectral lines of singly and doubly-ionized rare earth elements (REE), H $\alpha$ , H $\beta$ , O I, Fe I, Ca I, and Ba II.

The spectra were reduced using standard IRAF tasks. Each stellar, flat and calibration frame had a mean bias subtracted and

was then cleaned of cosmic ray hits and collapsed to one dimension. The spectra were divided by a mean flat-field, extracted in the same way, and the continuum was fitted with a three-segment cubic spline, using the same rejection parameters for all spectra so that the continuum fit is as uniform as possible.

The wavelength scale was established using about 40 lines of a ThAr emission lamp, resulting in an rms scatter of about  $3 \times 10^{-4}$  Å. The wavelength scale was linearly interpolated between ThAr lamp spectra taken before and after the stellar series, but the spectra were not sampled to a linear wavelength spacing.

### 2.2. Time-series of échelle spectra

- **SOFIN**: the observations from Nov. 6, 2003, were carried out with the SOFIN high resolution échelle spectrograph at the 2.56 m Nordic Optical Telescope (NOT), La Palma, Spain. Each spectrum had an integration time of 50 s with a readout time of 55 s, giving a time-resolution of 105 s. The typical  $S/N$  ratio is about 80 and the resolving power  $\approx 80\,000$ . These échelle spectra cover the region from 5000 to 6800 Å. The échelle images were reduced with the Advanced Acquisition, Archiving, and Analysis (4A) package written in C (Ilyin 2000).

The standard reduction sequence includes bias subtraction from the CCD overscan, photon noise estimation for the pixel variances, correction for the CCD fixed pattern noise using a master flat field (a sum of 100 exposures), subtraction of the scattered light determined from a 2D spline fit to the inter-order gaps. The spectral order position is found from the flat field image and subsequently adjusted for each échelle science frame. This step is followed by a weighted extraction of spectral orders with elimination of cosmic spikes based on a linear regression. The shape of the spectra and fringes in the red part of the CCD are corrected with a flat field spectrum smoothed with a spline fit. The wavelength calibration is based on about 1300 ThAr spectral lines collected from two successive images, using a 2D fit to them, taking also the time of exposures for calibration and science frames into account. A zero point correction had to be applied which resulted in a final RV error of about  $25 \text{ m s}^{-1}$  at the image center.

- **HARPS** and **UVES**: the 2004 spectroscopic observation were carried out with HARPS (High Accuracy Radial velocity Planet Searcher) spectrometer at the 3.6-m telescope at ESO, La Silla. 92 spectra with 60 s exposure time,  $S/N = 120$ , and 120 000 resolving power were taken during November 10/11, 2004, simultaneously with MOST. Because of the unique coincidence with the space photometry, Director’s Discretionary Time (274.D-5011) was granted for November 11/12 and 12/13 with the UVES spectrograph at the 8.2-m telescope, UT2 (Kueyen), of the VLT on Paranal, Chile, (92 and 73 spectra, 50 s exposure time,  $S/N = 300$ , with a resolving power of about 80 000).

All spectra were reduced and normalized to the continuum level with a routine specially developed by one of us (DL) for a fast reduction of time-series observations. It is a component of the spectral reduction package STAR XP, a special modification of the Vienna automatic pipeline for échelle spectra processing (Tsymbal et al. 2003). All bias and flat field images were median averaged before calibration. The scattered light was subtracted by using a 2D background approximation. For cleaning of cosmic rays we used a new algorithm which compares the direct and reversed spectral profiles. To determine the spectrum order boundaries, the code uses a special template for each order position in each row across the dispersion axis. The shift of the row spectra relative to the template is derived by a cross-correlation

**Table 1.** Journal of time-resolved spectroscopy of HD 24712. Listed are, among others, the duration of a continuous set of observations (Run, in hours) in a given night and the number of individual spectra taken during such a run, and the typical  $S/N$  ratio for the continuum.

Set No.	Civil date (UT)	Start HJD (2 450 000+)	Spectral range (Å)	Run (h)	No. of spectra	Exposure time (s)	Overhead time (s)	Typical $S/N$	Rot. phase	Instr.
1	2001.10.02	2 185.15654	6106–6189	3.77	123	60	42	100	0.71	GECKO
2	2001.10.03	2 186.15303	6106–6189	4.60	162	60	41	100	0.79	GECKO
3	2001.10.04	2 187.15230	6620–6730	4.77	163	60	42	100	0.87	GECKO
4	2002.09.23	2 541.08000	5822–5887	2.44	82	60	44	100	0.28	GECKO
5	2002.09.24	2 541.16417	6543–6658	1.43	49	60	44	100	0.29	GECKO
6	2002.09.24	2 542.02444	5822–5887	2.03	66	60	44	100	0.36	GECKO
7	2002.09.25	2 542.11958	5284–5344	1.96	66	60	44	100	0.37	GECKO
8	2002.09.25	2 543.05228	5822–5887	1.89	65	60	44	100	0.44	GECKO
9	2002.09.26	2 543.14946	6105–6195	1.84	64	60	44	100	0.45	GECKO
10	2002.09.26	2 544.14997	5822–5887	3.81	127	60	44	100	0.53	GECKO
11	2003.11.06	2 949.69312	4540–9952	1.58	53	50	55	80	0.08	SOFIN
12	2004.11.11	3 320.78693	3850–6730	2.31	92	60	30	120	0.87	HARPS
13	2004.11.12	3 321.74421	3400–6720	2.09	92	50	30	300	0.94	UVES
14	2004.11.13	3 322.77598	3400–6720	1.73	73	50	30	300	0.03	UVES
15	2004.11.15	3 324.60032	4575–7872	1.07	35	60	52	120	0.18	SARG
16	2004.12.02	3 341.66789	4575–7872	1.13	33	60	52	120	0.55	SARG

technique. Wavelength calibration was done by the usual 2D fit. The accuracy of this procedure is  $\approx 20 \text{ m s}^{-1}$ . The final step of continuum normalization was done by transforming of the flat field blaze function to the response function in each order.

- *SARG*: during MOST observations of HD 24712, additional spectra were obtained in Nov. 14/15, 2004, (35 spectra), and on Dec. 01/02, 2004, (33 spectra), with the high resolution spectrograph (SARG) at the 3.55-m *Telescopio Nazionale Galileo* (TNG) at the Observatorio del Roque de los Muchachos (La Palma, Spain). The spectra were reduced using standard ESO-MIDAS software with the same main steps as described above. The spectra cover the range of 4570–7900 Å, have a resolving power of about 57 000 and a  $S/N$  ratio of approximately 120. The time resolution was 129 s (60 s for exposure and 69 s for read out).

### 2.3. Polarimetry with SOFIN

The spectropolarimetric observations of HD 24712 were carried out between Oct. 29, and Nov. 18, 2003, with the high resolution échelle spectrograph, SOFIN, attached to the Cassegrain focus of NOT. The spectrograph is equipped with three different cameras offering three different resolving powers. To obtain observations in the polarimetric mode, the second camera with a resolving power of  $\approx 80 000$  was used. Between 4000–7000 Å seven spectral orders, each covering about 40 to 50 Å were used for the magnetic field analysis.

The circularly polarized spectra were obtained with a Stokesmeter, consisting of a fixed achromatic quarter-wave plate, a beam splitter made of a calcite plate, and an achromatic rotating quarter-wave plate, whose position is controlled by a stepping motor. To obtain accurate circular polarization measurements, usually a sequence of four exposures is obtained. Each of the beams is exposed twice, with the quarter-wave plate rotated by  $90^\circ$  after the first and before the last exposure. Such a sequence reduces instrumental effects to a minimum, because in the images taken with the quarter-wave plate rotated by  $90^\circ$ , instrumental signatures change sign and cancel when averaging the two exposures.

Data reduction was performed with the aforementioned 4A software package including all standard procedures, such as

**Table 2.** Journal of spectropolarimetric observations of HD 24712. The longitudinal field ( $\langle B_z \rangle$ ) was estimated using ten Nd II and Nd III lines (3rd column), and seven Cr I, Cr II, and Fe I lines (4th column).

HJD (2 450 000+)	Rotation phase	$\langle B_z \rangle$ (G)	
		Nd II, Nd III	Cr I, Cr II, Fe I
2 941.6516	0.44	$598 \pm 165$	$87 \pm 68$
2 943.6341	0.60	$909 \pm 154$	$240 \pm 132$
2 945.5758	0.76	$1109 \pm 105$	$535 \pm 145$
2 946.5973	0.84	$1090 \pm 144$	$729 \pm 180$
2 947.6067	0.92	$1182 \pm 100$	$1098 \pm 98$
2 948.6514	0.00	$1132 \pm 98$	$1064 \pm 130$
2 952.6267	0.32	$835 \pm 174$	$258 \pm 79$
2 953.6572	0.40	$629 \pm 129$	$155 \pm 86$
2 954.6316	0.48	$720 \pm 192$	$165 \pm 155$
2 955.6350	0.56	$830 \pm 187$	$137 \pm 107$
2 956.5954	0.64	$1062 \pm 178$	$260 \pm 174$
2 957.5958	0.72	$1159 \pm 164$	$483 \pm 158$
2 961.6160	0.04	$1168 \pm 100$	$1048 \pm 152$

bias subtraction, flat field correction, subtraction of the scattered light, weighted extraction of the orders, and bad pixel (cosmic ray) corrections. ThAr exposures obtained before and after each observing night were used to perform wavelength calibration and to test for possible spurious instrumental polarization, caused e.g. by bending of the spectrograph which is directly mounted on the telescope, different positions of the star on the slit, or temporal variations of the seeing.  $S/N$  ratios for the observed spectra are typically 200–300. Rotation phases of HD 24712 (see Table 2) were calculated according to the ephemeris and rotation period derived by Ryabchikova et al. (2005b).

### 3. Radial velocities and magnetic field strength

For radial velocity (RV) measurements we carefully chose unblended or minimally blended lines in the 3300–6800 Å spectral region. Between 3900 and 4400 Å the cores of the strong (resonance) lines of Ca, Fe and Sr were measured. Our choice was based on synthetic spectrum calculations over the whole spectral region of 3300–6800 Å, made with the spectral

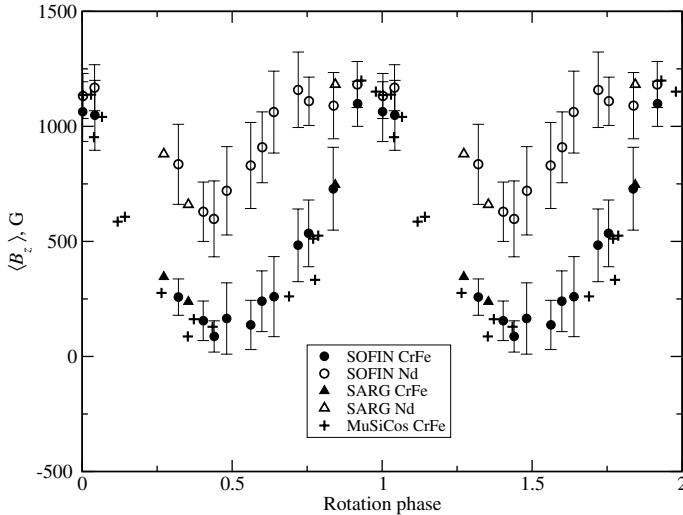


**Fig. 1.** Longitudinal magnetic field variations in HD 24712. Open (Nd lines) and filled (Cr-Fe lines) circles are the observations presented in this paper, open and filled triangles are magnetic measurements from Leone & Catanzaro (2004), and crosses represent data taken from Ryabchikova et al. (2005b).

synthesis code SYNTH3 written by Kochukhov, and using the atmospheric parameters and abundances from Ryabchikova et al. (1997). Atomic parameters of spectral lines for the synthesis were extracted from the Vienna Atomic Line Database, VALD (Kupka et al. 1999), and from the Database for Rare Earths at Mons University, DREAM (Biémont et al. 1999), which is also accessible via the VALD extraction procedures. For the Nd III identification additional atomic data from Crosswhite (1976), Aldenius (2001) and Ryabchikova et al. (2006) were used.

The radial velocities were measured with a center-of-gravity technique and attention was paid to the stability of the spectrographs. HARPS time-resolved spectra provide stable results with a mean rms dispersion of  $20 \text{ m s}^{-1}$  per individual non-pulsating line, while a quasi-linear, long-term drift was found in both nights of the observations with UVES. These drifts were approximated with a smooth spline function based on the average measurements of a few unblended non-pulsating Fe I lines. This quasi-linear drift was then subtracted from the RV measurements of all other spectral lines. It should be emphasized that the instrumental variation of the spectrograph’s zero point occurs on a much longer time scale than the stellar  $p$ -mode variability, and therefore does not affect the pulsation analysis presented here.

Radial velocities of more than 500 unblended spectral lines were measured in the spectral region from 3900 to 6800 Å, and additional 80 lines were measured in the region blueward the Balmer jump (BJ). A complete list of measured lines (but not all individual measurements) together with their identification is given in Table 4 (Online material). The purpose of this table is to provide line identifications and to indicate pulsating and non-pulsating lines.

The longitudinal magnetic field was measured as the first moment of the observed Stokes  $V$  parameter for a set of chosen spectral lines. We have performed separate measurements of the iron-peak elements (Cr and Fe) and of the REEs (Nd and Tb). The results and error estimates are given in Table 2 and are illustrated in Fig. 1. For a comparison,  $\langle B_z \rangle$  data from Ryabchikova et al. (2005b – MuSiCos) and from Leone & Catanzaro (2004 – SARG) are also included in this figure.

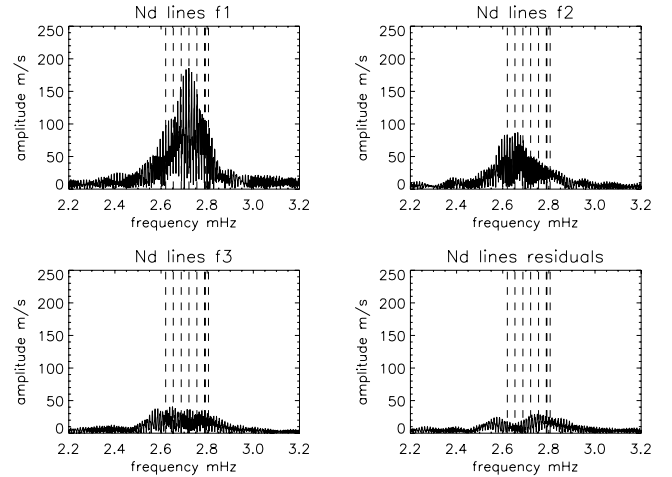


**Fig. 2.** Amplitude spectra of the Nd III spectral lines of the 2004 observations. The *top left panel* shows the DFT of the original RV data; the *top right panel* represents the DFT after prewhitening with the highest amplitude frequency; the *other panels* show the next prewhitening steps. Dashed lines indicate photometric frequencies according to Kurtz et al. (2005).

We found that some spectral lines with large Landé factors are partially split in non-polarized spectra. In particular one line, Cr I 5247.56 Å, is a pure triplet with  $g_{\text{eff}} = 2.51$ , and another line, Fe II 6432.48 Å, is a pseudo-doublet with  $g_{\text{eff}} = 1.82$ . Using these lines we estimated the magnetic modulus  $\langle B \rangle$  at phases 0.867, 0.944 (close to the magnetic maximum) and at phase 0.42 (near the magnetic minimum). For the latter, a UVES spectrum of HD 24712 was extracted from the ESO archive.  $\langle B \rangle$  estimates were made by fitting calculated synthetic line profiles to the observed spectra. Magnetic synthetic calculations were carried out with SYNTHMAG (Kochukhov 2006), which represents an improved version of the program described by Piskunov (1999).  $\langle B \rangle$  varies between 3100–3300 G at  $\langle B_z \rangle_{\text{max}}$  and 2500 G at  $\langle B_z \rangle_{\text{min}}$  according to our estimates.

#### 4. Frequency analysis

Although RV variations in the REE lines due to pulsation are very distinctive and the relative accuracy of individual spectroscopic data is higher than for photometry, it proved to be difficult to study in detail the frequencies of multiperiodic roAp stars by spectroscopy, because a large telescope is needed during an extended period of time. For a reliable frequency analysis it is necessary to observe continuously during weeks with a minimum of gaps. This is possible either with dedicated satellites, as is MOST for photometry, or with multisite ground based campaigns, such as WET (Kurtz et al. 2005). Although our spectroscopic monitoring does not allow for a detailed frequency analysis, we performed nevertheless such an analysis to confirm the consistency of the main frequencies in the spectroscopy obtained simultaneously with the MOST photometry.

Our Fourier analysis of the RV data of selected lines – Pr III 5284, 5300 Å, Nd III 5203, 5294, 5845, 5851, 5987, 6145 Å and Tb III 5505 Å – was based on a discrete Fourier transform (DFT) and stepwise prewhitening with a sine fit to the highest amplitudes (see Fig. 2). In this analysis we used all spectra obtained simultaneously with MOST during four nights around the magnetic maximum (sets 12 to 15). The duty cycle for this combined 4-night data set is poor (about 8%), but knowing

from MOST photometry which alias to avoid, we found the 3 highest amplitude periods in our spectroscopy to be 6.125 min, 6.282 min, and 6.202 min. These values agree well with contemporaneous MOST photometry, as is illustrated in Fig. 3 for one of the pulsating lines (Pr III 5300 Å). These frequencies correspond to  $\nu_4$ ,  $\nu_2$ , and  $\nu_3$  in Kurtz et al. (2005). The frequency analysis performed for the 2001 Nd III data gives two main frequencies  $\nu_4$  and  $\nu_2$  (identification according to Kurtz et al., op. cit.) with similar amplitudes as in 2004 (see Fig. 9 in Online Material). This figure illustrates (as does Fig. 2) the possibility to identify pulsation frequencies, amplitudes and phases even in short spectroscopic runs distributed over several nights – what results in a very poor duty cycle – provided one can avoid aliases thanks to MOST and WET photometry.

The short observing run in 2003 does not allow us to resolve frequencies. Only one frequency close to  $\nu_3$  was derived.

Different authors prefer to characterize periodic signal either with periods or with frequencies. For convenience of the reader we mention here the conversion: period in minutes transforms to a frequency in mHz via  $\nu(\text{mHz}) = 16.6667/P(\text{min})$ .

## 5. Phase relations between photometry and spectroscopy

Our time-resolved observations in 2004 were carried out simultaneously with the Canadian micro-satellite MOST which monitored HD 24712 from 2004 November 6, to December 5. This provides us with the opportunity to derive directly the phase lag between photometry and spectroscopy.

This was attempted already earlier by Matthews et al. (1988) despite a rather poor  $S/N$  ratio ( $\approx 20$ ) of their individual spectra. But the large number of spectra ( $\approx 600$ ) allowed the authors to derive an average RV curve and to find a coincidence of RV maxima with  $\delta B$  minima, which corresponds to a phase lag of about 0.5, where we define a phase lag as a phase difference between the maxima of both, photometric and RV variations. They found the photometric maximum to occur typically *after* the RV maximum, which we confirm with our data.

The high  $S/N$  and spectral resolution of the present observations resulted in more precise values for phase lags, and in particular it allowed us to determine this quantity for individual spectral lines. In order to minimize the influence of the higher point-to-point scatter of the photometric data with respect to the spectroscopic observations, we computed an artificial time-series data set based on the 3 dominant frequencies and their amplitudes and phases ( $\nu_2$ ,  $\nu_3$  and  $\nu_4$ ) which were derived from the complete set of MOST observations. Next, this artificial time-series was cross-correlated with the RV observations of the individual spectral lines. The time interval for the cross correlation ranges from plus to minus 6.125 min, the latter corresponds to the period with the largest amplitude ( $\nu_4$ ). The time step was 1 s. The best correlation gives the time lag between photometry and spectroscopy expressed in seconds.

The time lags obtained with artificial time-series data generated with the 3 dominant frequencies differ only by  $\sim 2$  s from those obtained with a full set of frequencies which is about an order of magnitude less than the accuracy of the used correlation technique. The remaining frequencies in the full MOST frequency solution with very low amplitudes obviously do not affect the time lag determination.

In Fig. 3 we illustrate the excellent agreement between the RV variations of the Pr III spectral line and the photometric observations, shifted by about  $-197$  s, which corresponds to a phase

lag of  $-0.54$ , using the main photometric pulsation frequency. Both observations are normalized and scaled for better visibility.

The result of the cross-correlation procedure is given in Table 3. The brightness maximum occurs for all lines after the RV maximum, but the phase lag itself depends strongly on the individual line. It is largest for the H $\beta$  line, which has a minimal RV amplitude of  $91 \text{ m s}^{-1}$ , and gradually decreases for lines showing higher amplitudes. It will be shown in a following paper that this gradual change in phase lag is probably connected with line formation in the atmosphere.

## 6. Radial velocity variations of individual elements

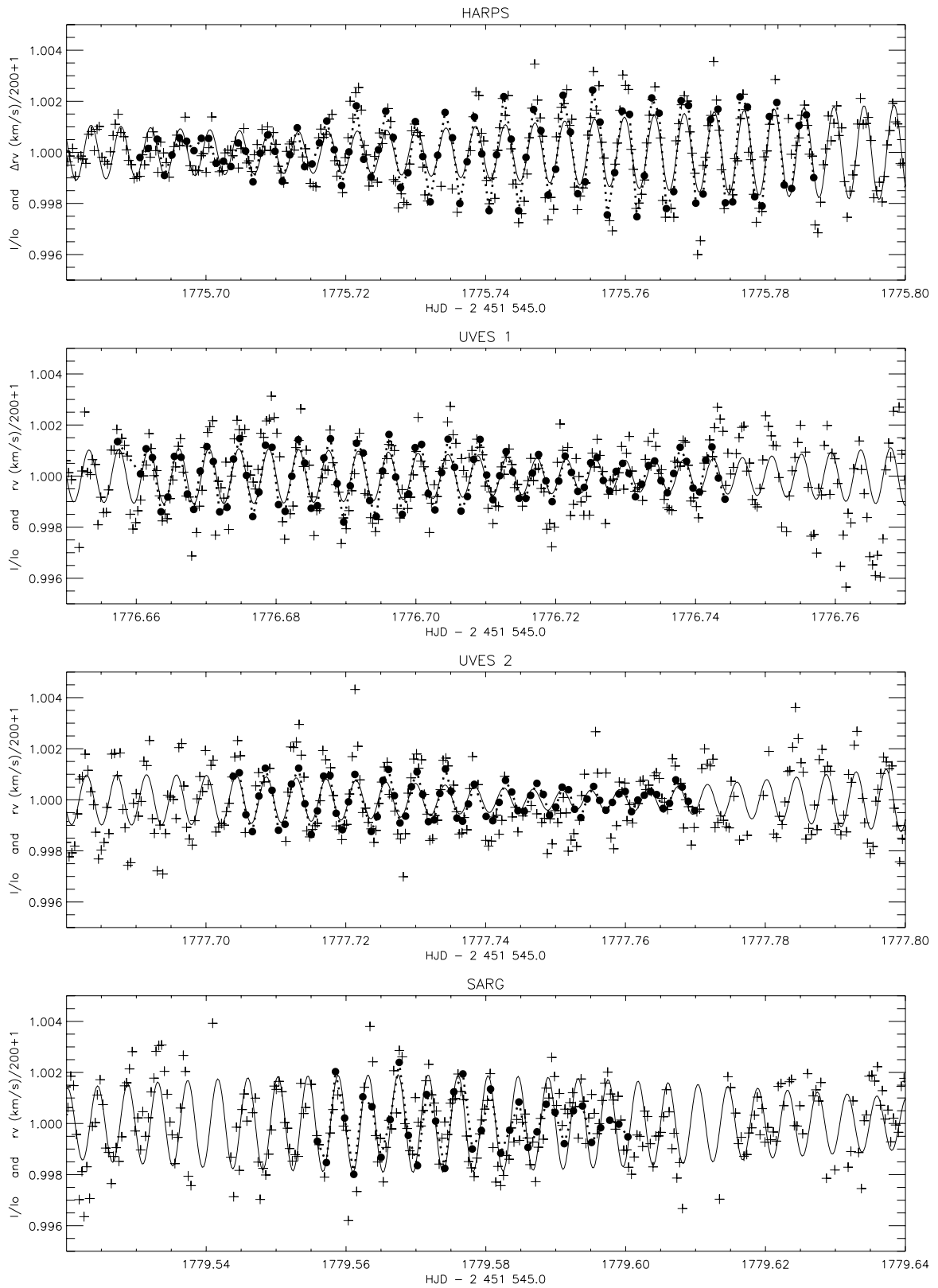
For all measured lines we did a period search with the periodogram method. This analysis allowed us to crudely estimate the probability that a given period is true (Horne & Baliunas 1986). They developed an algorithm which applies to fully resolved frequency spectra. The results – RV amplitudes with the error, period and error, and probability of the period – are given in Table 4 (Online Material). HJD = 2 453 320.0 was chosen as a reference time for our pulsation analysis. It is remarkable that the weighted mean from all periods with a probability higher than 0.99 determined from individual lines yields exactly the value of the most prominent photometric period observed in 2000–2004, which is  $P = 6.125$  min.

The large number of measurable lines of different chemical species allows for a detailed analysis of pulsation waves in the atmosphere of HD 24712, but which will be presented in a follow up paper. Here we discuss briefly pulsation properties derived for different chemical elements.

- *Hydrogen:* H $\gamma$ , H $\beta$  and H $\alpha$  cores indicate pulsation with the amplitude increasing from H $\gamma$  to H $\alpha$ . Our measurements support the results obtained by Balona & Laney (2002) for  $\alpha$  Cir and by Balona (2002) for HR 3831, and all together they provide a direct evidence for the growth of pulsation amplitudes towards the upper atmospheric layers. Bisector measurements of the H $\alpha$  line are shown in Fig. 4 (RV amplitudes – right panel, phases – left panel). Both, amplitudes and phases increase with line depth, i.e. towards the upper atmospheric layers as is observed also in other roAp stars (for example  $\alpha$  Cir, Baldry et al. 1999;  $\gamma$  Equ, Sachkov et al. 2004a; or HD 99563, Elkin et al. 2005).

- *Na, Mg, S and Si:* lines of these elements do not reveal any pulsation. The upper limit for the RV amplitudes ranges from  $10$  to  $30 \text{ m s}^{-1}$ , depending on the line strength and hence accuracy of measurements. Bisector measurements across the Mg I 5172 Å line (Fig. 5) also rejects variability with an amplitude above  $40 \text{ m s}^{-1}$ . With the exception of the bisector close to the continuum ( $r = 0.96$ ) we never recover the true pulsation period in a periodogram. The pulsation signal at  $r = 0.96$  is explained by a La II blend in the red wing of the Mg I line. A significant pulsation amplitude was also measured in the 4696.20 Å line, which coincides with a S I feature, but which may be attributed to an unclassified Nd III line at  $\lambda 4696.205$  Å. The latter information is from the unpublished lists of Crosswhite (1976) which were the main source for official NIST data on Nd III energy levels (Martin et al. 1978).

- *Fe-peak elements:* about half of the measured Ca lines show oscillations compatible with the photometrically observed pulsation periods. In four cases we found a signal with 96% significance, among which is the core of the resonance Ca II 3933 Å line, obviously formed high in the atmosphere. Bisector measurements across the Ca I 6122.22 Å line are shown in Fig. 5.

PR3\_5299: phot. signal shifted about  $-197\text{sec.}$  ( $\phi = -0.536$ )

**Fig. 3.** Normalized RV variations for Pr III (filled circles) are compared with a synthetic light curve (black solid line, computed with the three largest amplitude frequencies derived from the entire MOST observing run) and with simultaneous MOST photometric data (crosses). The dotted line connects the Pr III 5299 Å spectral line RV values (dots) and it follows well the solid line, based on MOST photometry.

**Table 3.** Phase lag in seconds between luminosity and RV variations for different chemical species. The fourth column gives the same phase lags based on a pulsation period of 6.125 min.

Line	$\lambda$ (Å)	Phase lag	
		in seconds	in periods
H $\beta$	4861	$-356 \pm 25$	$-0.97 \pm 0.08$
Eu II	6645	$-356 \pm 22$	$-0.97 \pm 0.06$
Nd II	6650	$-313 \pm 22$	$-0.85 \pm 0.06$
H $\alpha$	6563	$-307 \pm 22$	$-0.84 \pm 0.06$
Nd III	5286	$-301 \pm 21$	$-0.82 \pm 0.06$
Nd II	5255	$-297 \pm 21$	$-0.81 \pm 0.06$
Nd III	6690	$-294 \pm 22$	$-0.80 \pm 0.06$
Nd III	5851	$-283 \pm 22$	$-0.77 \pm 0.06$
Dy III	5730	$-278 \pm 22$	$-0.76 \pm 0.06$
Nd III	5845	$-270 \pm 21$	$-0.73 \pm 0.06$
Nd III	5203	$-255 \pm 21$	$-0.69 \pm 0.06$
Nd III	5294	$-247 \pm 22$	$-0.67 \pm 0.06$
Pr III	5300	$-197 \pm 21$	$-0.54 \pm 0.06$
Tb III	5505	$-104 \pm 22$	$-0.28 \pm 0.06$

Although this line indicates weak variation with a period of 6.125 min (and a probability of 0.82%), the bisector variations do not differ from those of constant Mg I and Fe II lines. A small unknown blend of a REE would be enough to produce a spurious, very low amplitude variation in even a strong, but non-pulsating line (see below).

Three out of 5 Sc II lines show pulsation, but they all are blended with REE lines. Similarly, nine out of 21 measurable Ti lines show small amplitude variations with the known pulsation period. The Ti II 4501.26 Å line is blended with Nd III 4501.23 Å which contributes to about 25% of the total line intensity, thus resulting in the pulsation signal with the typical phase of Nd lines.

Cr, Mn, Fe, and Co lines do not pulsate. Only 25% of the whole set of measured lines have pulsation periods typical for HD 24712, and part of these lines are blended with lines of REEs. Figure 6 displays RV amplitudes derived from sine-fits to lines of Fe-peak elements with a pulsation period of 6.125 min, and as a function of central residual intensities. We can conclude the absence of pulsation with amplitudes exceeding  $15 \text{ m s}^{-1}$  in the whole atmospheric range where Fe-peak lines are formed. An apparent increase of the RV amplitude for weaker lines simply reflects a reduced accuracy of the measurements.

A few lines of the Fe-peak elements have rather large RV amplitudes (triangles in Fig. 6) and in most cases this is a result of blending with a REE. Two spectral lines at 5208 Å and 5429 Å are of particular interest, because they are usually identified as Cr I and Fe I lines, respectively, and their pulsation characteristics attributed to these elements (e.g., Elkin et al. 2005). Actually, these lines are heavily blended with Pr III 5208 Å and Nd III 5429 Å, respectively, and consequently show typical REE pulsation phases, but with reduced amplitudes.

• *Sr to Ba*: spectral lines of Sr, Y, Zr, Rh, Pd, In and Ba were measured in the spectrum of HD 24712. Five Ba II lines are constant to within  $10 \text{ m s}^{-1}$ , as are also lines of Rh I and Pd I. A spectral feature at  $\lambda 4511.26 \text{ Å}$ , identified as In I 4511.31 Å, may be blended with an unclassified line of Ho (Crosswhite 1976). Pulsation is seen in Sr II lines and in five out of 11 lines of Y II. We carefully checked for blends and can exclude this possibility as explanation for a pulsation signal. Pulsation does not appear in weaker lines of Y II and there is a definite dependence of the RV amplitude and phase on line intensity. It seems that Y II lines

originate in the atmosphere where lines with high pulsation amplitudes just start to be formed.

• *Rare Earth elements*: we have measured 260 lines of 13 REEs in the first and the second ionization stage. Almost all of them show pulsation with large amplitudes and different pulsation phases, depending on the species and line intensity (see also Table 3). Bisector measurements at different (continuum normalized) intensity levels of two representative lines, Nd III 5294 Å and Pr III 5300 Å, are shown in Fig. 4. Although RV variations are present, they are not as large as in the roAp star  $\gamma$  Equ (Sachkov et al. 2004a). No difference in the pulsation signature is found for lines of the same element/ion located on both sides of the Balmer jump. For example, two Nd III spectral lines,  $\lambda 3603$  and  $\lambda 6145 \text{ Å}$ , formed at approximately the same depth in the stellar atmosphere according to Mashonkina et al. (2005) have RV amplitudes of 185 and  $194 \text{ m s}^{-1}$ , and pulsation phases of 0.74 and 0.79, respectively (data set 13, UVES).

• *Thorium*: two lines identified as Th III were measured, but no significant pulsation was detected. Using equivalent width measurements and the model atmosphere from Ryabchikova et al. (1997), we estimate a Th abundance of  $\log(\text{Th}/N_{\text{tot}}) = -9.26 \pm 0.12$ . Oscillator strengths for Th III lines were taken from Biémont et al. (2002). The thorium abundance in HD 24712 is comparable to that in HD 101065 (Cowley et al. 2000), and the thorium overabundance in the atmosphere is similar to the overabundance of most REE obtained from the first ions. Note, that Th abundance in both stars, HD 24712 and in HD 101065 has been derived using partition functions (PF) from Kurucz' ATLAS9 code.

• *Unidentified lines*: along with lines of well established identification we measured all unidentified features with equivalent width  $\geq 10 \text{ mÅ}$ . The total number of these lines is 115, and about one third of them coincide with the position of Nd III lines from Crosswhite's unpublished list. Because they are not yet classified, we consider them as unidentified lines requiring a proper identification. Most of these potential Nd III lines have pulsation phases in the range of 0.4 to 0.5, corresponding well to the classified Nd III lines. Only one line at  $\lambda 4748.17 \text{ Å}$  does not show pulsation variations, all other lines reveal pulsation with the typical amplitudes and phases of REEs. We conclude that plenty of still unknown REE lines are present in the spectra of roAp stars.

The ability to constrain classification of unidentified lines on the basis of their pulsation amplitudes and phases and thus provide useful information for laboratory studies is worth mentioning. This is a unique property of roAp stars, and it was already used in the classification study of the Nd III lines (Ryabchikova et al. 2006).

## 7. Discussion

We have obtained time-resolved observations with different spectrographs in different years (2001, 2003 and 2004) and at nearly the same rotation phases close to the magnetic maximum. We have already reported the similarity of phase shifts between RV variations in the lines of different elements/ions (Sachkov et al. 2004b) based on the observations taken in 2001 and 2003. Figure 7 gives another comparison of the RV variations derived from the observations taken in 2001 (GECKO) and in 2004 (HARPS) at rotation phase 0.87. It was mentioned in Sect. 4 that the frequency analysis of our observations in 2001 and 2004 reveals the same highest amplitude frequencies of 2720.9 and  $2652.9 \mu\text{Hz}$ , which corresponds to pulsation periods

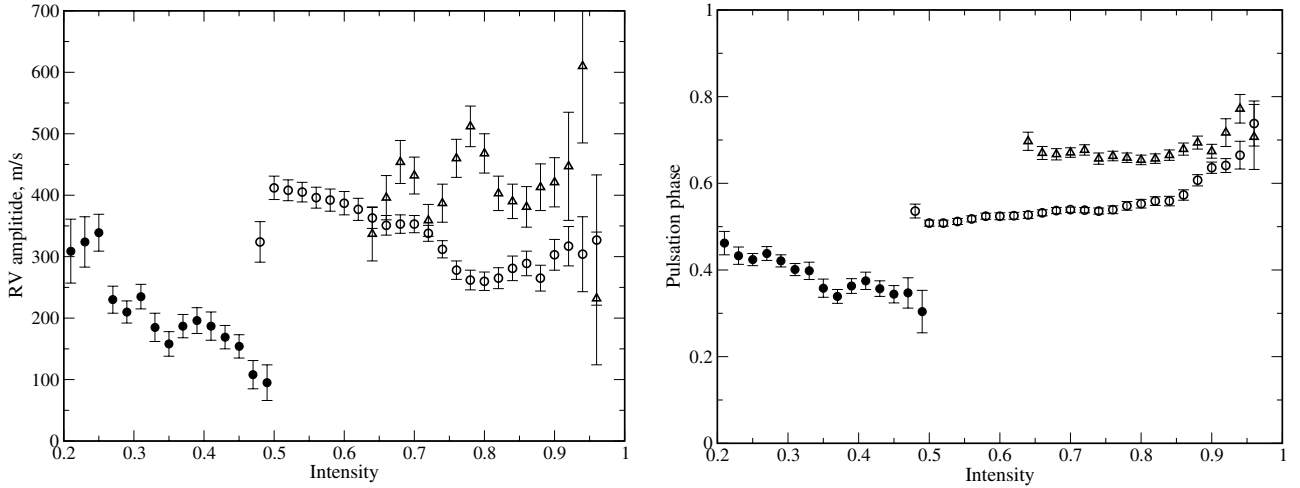


**Fig. 4.** Bisector measurements of the  $H\alpha$  line (filled circles), lines of Nd III 5294 Å (open circles), Pr III 5300 Å (open triangles), (crosses). The RV amplitudes are shown in the *left panel* and pulsation phases (based on  $P = 6.125$  min) in the *right panel*.

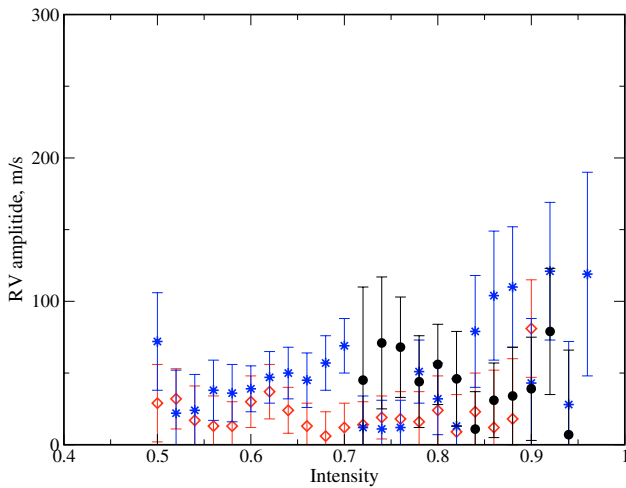


**Fig. 5.** Bisector RV amplitudes (based on  $P = 6.125$  min) of Fe II 5169 Å (open diamonds), Mg I 5172 Å (asterisks), and Ca I 6122 Å (filled circles).

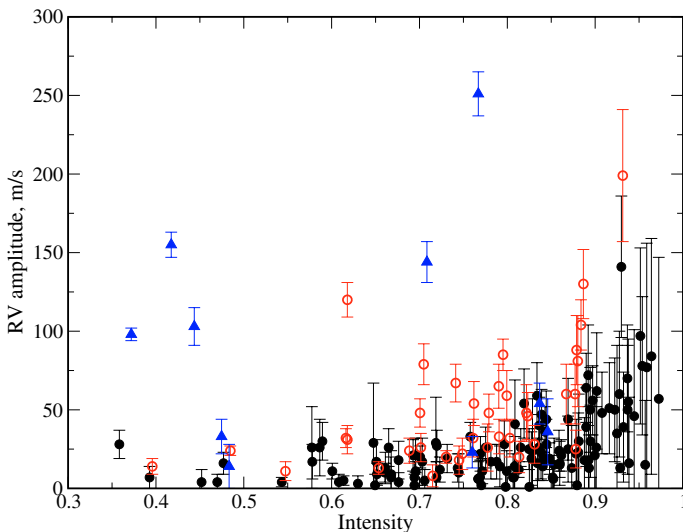


**Fig. 6.** Pulsation amplitude versus central residual intensity for lines of Fe-peak elements. Filled/open circles indicate lines with no pulsation/known pulsation period, respectively. Fe-peak lines known to be blended with the REEs are marked with triangles.

of 6.125 and 6.28 min. In 2003 we got only 53 spectra and hence we can not resolve frequencies, therefore a mean period of 6.20 min was used. RV amplitudes and phases for a sample of common lines observed in 2001, 2003 and 2004 are given in Table 5 (Online material). Phases in 2001 and 2003 were calculated relative to the HJD of the first observation in a given year and were shifted for comparison purpose by  $-0.1$  and  $-0.2$ , respectively. Obviously, the same lines are variable and the similarity of amplitudes and phases of the RV maximum indicate stability of the pulsation pattern in the atmosphere of HD 24712 at least during recent years.

Simultaneous photometry and spectroscopy allow us for the first time to phase accurately RV variations due to pulsation observed in different spectral lines with the photometric pulsation signature. To determine a phase shift between RV and light variations we used the pulsation frequency with the largest photometric amplitude in the WET and MOST data (6.125 min).

Our results show a gradual decrease of the phase lag from the  $H\beta$  line to Tb III lines, which may be interpreted as a running wave in the atmosphere of HD 24712, if different lines are formed at different atmospheric layers. The same phenomenon, known as the Van Hoof effect, was found earlier in  $\beta$  Cep-type stars (Mathias & Gillet 1993) and allowed them to derive the propagation time of the running wave through the stellar atmosphere. A first estimate of the running pulsation wave speed in the atmosphere of HD 24712 can be obtained from the phase lags and the respective formation depths of the Nd II and Nd III lines determined according to Mashonkina et al. (2005). In the relevant atmospheric layers ( $-6.2 \leq \log \tau_{5000} \leq -4.2$ ) the pulsation wave propagates with nearly constant speed of  $\sim 6 \text{ km s}^{-1}$  which is slightly less than the sound speed in adiabatic approximation.

An analysis of the running wave properties in a roAp star atmosphere is rather difficult. First, we know that elements are stratified in the atmospheres of Ap and roAp stars (Babel 1992; Ryabchikova et al. 2002, 2005a), and therefore stratification has to be taken into account for the line formation depth calculations. Second, a stratification analysis of the REEs, which are the main carriers of pulsation information, is not correct without considering NLTE effects (Mashonkina et al. 2005). The third important issue is the surface inhomogeneity in the chemical composition. HD 24712 is a spectrum variable and the first rough analysis of the element distribution was published by Preston (1972). Later, Ryabchikova et al. (2000) showed evidence for a concentration



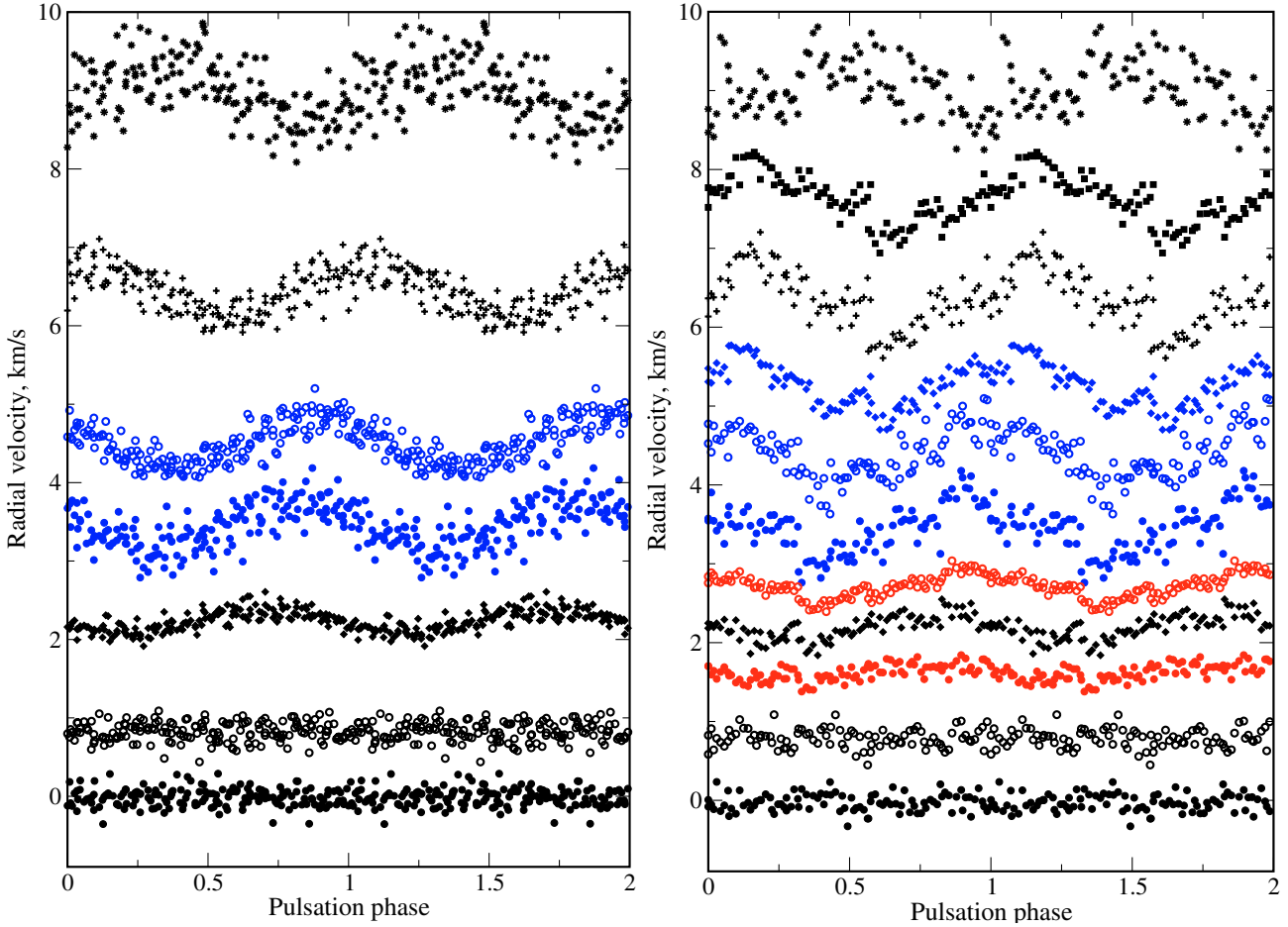


**Fig. 7.** Radial velocity variations with a period of  $P = 6.125$  min for selected spectral lines in 2001 (*left panel*) and in 2004 (*right panel*). In the right panel lines from bottom to top are: Ca I 6717, Fe I 6678, H $\beta$  (core), Eu II 6645, H $\alpha$  (core), Nd II 6650, Nd III 6690, Nd III 6550, Pr III 6706, Er III 4735, and Tb III 6688 Å. Same lines except of H $\beta$  (core), H $\alpha$  (core), Nd III 6550, and Er III 4735 are displayed in the *left panel*.

of the Fe-peak elements in a wide band around the magnetic equator, while REEs (in particular Pr and Nd) and Co are concentrated in large spots near, but not exactly at one magnetic pole (the other pole is never visible). Our magnetic field measurements support this difference in the element surface distribution.

Recent Magnetic Doppler Imaging of HD 24712 (Lüftinger et al. 2006) revealed a small but non negligible difference (both in longitude and latitude) between the surface distributions of different REE elements. Therefore, part of the phase shifts between RV curves *may* be due to the different chemical surface distribution relative to the magnetic pole. Cunha (2006) showed that phase shifts may reach 0.25 of the period between the magnetic pole and the magnetic co-latitude  $\theta \sim 30^\circ$  (see lower panel of Fig. 6 in Cunha 2006).

A detailed study of the line formation depth in the atmosphere of HD 24712 will be subject of a forthcoming paper. However, some first information may be obtained already without such a detailed analysis when plotting the maximum RV value observed for a given spectral line as a function of pulsation phase, determined from photometry. If the photometric pulsation phase of the maximum RV is related to specific line-forming layers in the stellar atmosphere, then we expect new insights in a pulsating atmosphere. Figure 8 shows RV amplitudes as a function of pulsation phases for numerous lines of several elements measured in UVES spectra (rotation phase 0.944). These pulsation data include bisector measurements of the H $\alpha$  core and the cores of Ca I and Ca II resonance lines.

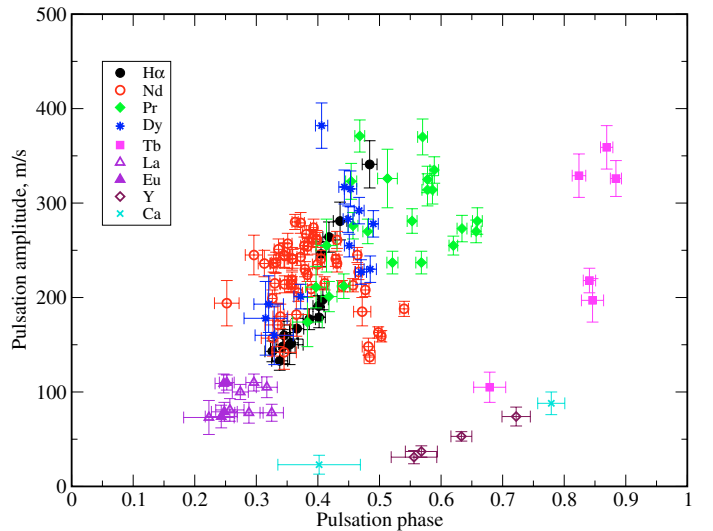


**Fig. 8.** Pulsation amplitude of spectral lines versus pulsation phase at RV maximum, based on a pulsation period of 6.125 min.

The data seem to cluster along two curves separated roughly by 0.5 of a pulsation period (Fig. 8). The first curve may be directly connected with optical depth, thanks to NLTE calculations for hydrogen and Nd lines (Mashonkina et al. 2005; Sachkov et al. 2006). The RV amplitude grows towards the

upper layers, reaches a maximum and then decreases, as indicated by the Nd and Pr lines.

At present it is difficult to conclude if the second curve represents another part of a continuous amplitude-phase distribution, because it is defined mainly by Y and Tb lines, which formation depths are unknown. We think that Tb lines are formed at about the same depth or higher than Nd, Pr and other REE lines. The core of the resonance Ca II 3933 Å line (pulsation phase of 0.8) may be also formed high in the atmosphere, particularly if one considers possible stratification of Ca. But the Y lines are probably formed in lower atmospheric layers.

Our observations allow us to check the claimed pulsation phase jumps of 180° at rotation phases corresponding to magnetic extrema (Mkrtychian & Hatzes 2005). These authors had to link two sets of observations, separated by one month (more than 9000 pulsation cycles), to cover these phases. The phase jumps reported by Mkrtychian & Hatzes occur exactly between the two sets of observations. We, on the other hand, do not observe any phase changes exceeding 35° (0.1 of the pulsation period) in our data sets, which fortunately happen to cover in 2002 the magnetic minimum in 4 consecutive nights (sets 4 to 10) and in 2004 the magnetic maximum in 4 nights of which three were consecutive (sets 12 to 15). Thus, we believe that the rotational modulation of pulsation phase reported for HD 24712 by Mkrtychian & Hatzes (2005) is spurious.

Finally we want to point again to Table 4 which provides the basis for the present investigation. It is a compilation of unblended spectral lines measured in the spectral range from  $\lambda$  3900 to 6800 Å and of further 80 lines bluewards the Balmer jump. Because of its volume this table is available only as on-line material. We present the measured central wavelengths of nearly 600 spectral lines in Å, followed by the pulsation amplitude in  $\text{m s}^{-1}$  and the amplitude error, the period with the largest amplitude determined with a least-squares fit after a periodogram analysis and the probability of the given period (Horne & Baliunas 1986). The next four columns give amplitude, amplitude error, phase relative to the main photometric period observed by MOST (6.125 min) and the phase error. These data are followed by the same information, but relative to the third prominent photometric period observed by MOST (6.282 min), which is the second prominent spectroscopic period. And finally we give in the last column additional information. This table includes information of pulsation properties of ~600 spectral lines in the roAp star HD 24712 observed in 2004 in a range of more than 3000 Å. Because of the known rotational modulation of the pulsation RV amplitudes (see Fig. 3) the lines measured in both observing runs have different amplitudes in Table 4.

## 8. Conclusions

An extensive spectroscopic and polarimetric study of HD 24712 provide new information about the pulsation properties of a roAp star atmosphere. With this new analysis we confirm our previous results (Sachkov et al. 2004b) and of Balona & Zima (2002), that REE lines and the H $\alpha$  core show large pulsation amplitudes (150 to 400  $\text{m s}^{-1}$ ), while spectral lines of the other elements (Mg, Si, Ca, Fe-peak) are nearly constant.

Our data permit for the first time to determine directly the phase shifts for different chemical elements, respectively ions, between pulsation signatures observed in RV data and in photometry. These shifts, derived from contemporaneous photometric and spectroscopic observations, together with magnetic field

measurements over a stellar rotation period, will be used in our forthcoming structural analysis of the pulsating atmosphere of HD 24712.

*Acknowledgements.* We thank the MOST Science Team for providing us with the photometric data and frequency analysis of HD 24712 prior to publication. This work was supported by the Austrian FFG-ALR (MOST Ground Station) and Austrian Science Fund (FWF-P17580N2), by grant 11630102 from the Royal Swedish Academy of Sciences, and by the Natural Sciences and Engineering Research Council of Canada. T.R. and M.S. acknowledge financial support from RFBF grant 04-02-16788a and from the RAS Presidium (Program “Origin and Evolution of Stars and Galaxies”). We also thank our referee, Don W. Kurtz, for his constructive comments which helped to improve the paper.

## References

- Aldenius, M. 2001, Master Thesis, Depart. of Physics, Univ. of Lund  
 Babel, J. 1992, *A&A*, 258, 449  
 Baldry, I. K., Viskum, M., Bedding, T. R., et al. 1999, *MNRAS*, 302, 381  
 Balona, L. A. 2002, *MNRAS*, 337, 1059  
 Balona, L. A., & Zima, W. 2002, *MNRAS*, 336, 873  
 Balona, L. A., & Laney, C. D. 2003, *MNRAS*, 344, 242  
 Biémont, E., Palmeri, P., & Quinet, P. 1999, *Ap&SS*, 635, 269  
 Biémont, E., Palmeri, P., Quinet, P., Zhang, Z. G., & Svanberg S. 2002, *ApJ*, 567, 1276  
 Crosswhite, H. 1976, unpublished data  
 Cowley, C. R., Ryabchikova, T., Kupka, F., et al. 2000, *MNRAS*, 317, 299  
 Cunha, M. S. 2006, *MNRAS*, 365, 153  
 Cunha, M. S., Fernandes J. M. M. B., Monteiro, M. J. P. F. G. 2003, *MNRAS*, 343, 831  
 Elkin, V. G., Kurtz, D. W., & Mathys, G. 2005, *MNRAS*, 364, 864  
 Horne, J. H., Baliunas, S. L. 1986, *ApJ*, 302, 757  
 Ilyin, I. V. 2000, High resolution SOFIN CCD échelle spectroscopy, Ph.D. Thesis, University of Oulu  
 Kochukhov, O. 2006, in *Magnetic Stars*, ed. I. I. Romanyuk, & D. O. Kudryavtsev, in press  
 Kupka, F., Piskunov, N., Ryabchikova, T. A., Stempels, H. C., & Weiss, W. W. 1999, *A&AS*, 138, 119  
 Kurtz, D. W. 1982, *MNRAS*, 200, 807  
 Kurtz, D. W., Kawaler, S. D., Riddle, R. L., et al. 2002, *MNRAS*, 330, L57  
 Kurtz, D. W., Cameron, C., Cunha, M. S. et al. 2005, *MNRAS*, 358, 651  
 Leone, F., & Catanzaro, G. 2004, *A&A*, 425, 271  
 Lüftinger, T., Kochukhov, O., Ryabchikova, T., Weiss, W. W., & Ilyin, I. 2006, in *Magnetic Stars*, ed. I. I. Romanyuk and D. O. Kudryavtsev, in press  
 Martin, W. C., Zalubas, R., & Hagan, L. 1978, NSRDS-NBS 60, Washington  
 Mashonkina, L. I., Ryabchikova, T. A., & Ryabtsev, A. N. 2005, *A&A*, 441, 309  
 Mathias, P., & Gillet, D. 1993, *A&A*, 278, 511  
 Matthews, J. M., Wehlau, W. H., Walker, G. A. H., & Yang, S. 1988, *ApJ*, 324, 1099  
 Mkrtychian, D. E., & Hatzes, A. P. 2005, *A&A*, 430, 263  
 Preston, G. W. 1972, *ApJ*, 175, 465  
 Piskunov, N. E. 1999, in 2nd International Workshop on Solar Polarization, ed. K. Nagendra, & J. Stenflo, (Kluwer Acad. Publ.) *ASSL*, 243, 515  
 Ryabchikova, T. A., Landstreet, J. D., Gelbmann, M. J., et al. 1997, *A&A*, 327, 1137  
 Ryabchikova, T. A., Tsymbal, V. V., Malanushenko, V. P., & Savanov, I. S. 2000, in *Magnetic Fields of Chemically Peculiar and Related Stars*, ed. Yu. V. Glagolevskij, & I. I. Romanyuk, Moscow, 180  
 Ryabchikova, T., Piskunov, N., Kochukhov, O., et al. 2002, *A&A*, 384, 545  
 Ryabchikova, T., Leone, F., & Kochukhov, O. 2005a, *A&A*, 438, 973  
 Ryabchikova, T., Wade, G. A., Aurière, M., et al. 2005b, *A&A*, 429, L55  
 Ryabchikova, T., Ryabtsev, A., Kochukhov, O., & Bagnulo, S. 2006, *A&A*, 456, 329  
 Sachkov, M., Ryabchikova, T., Kochukhov, O., et al. 2004a, in *Variable Stars in the Local Group*, ed. D. W. Kurtz, & K. R. Pollard, *ASP Conf. Ser.*, 310, 208  
 Sachkov, M., Ryabchikova, T., Ilyin, I., et al. 2004b, in *The A-Star Puzzle*, ed. J. Zverko, W. W. Weiss, J. Žižňovský, & S. J. Adelman (Cambridge University Press), *IAU Symp.*, 224, 770  
 Sachkov, M., Ryabchikova, T., Bagnulo, S., et al. 2006, in *Stellar Pulsation and Evolution*, ed. A. R. Walker, G. Bono, *Mem. Soc. Astron. Ital.*, 77, 397  
 Tsymbal, V., Lyashko, D., & Weiss, W. W. 2003, in *Modelling of Stellar Atmospheres*, ed. N. Piskunov, W. W. Weiss, D. F. Gray, *ASP, IAU Symp.*, 210, E49  
 Walker, G., Matthews, G., Kuschnig, R., et al. 2003, *PASP*, 115, 1023

# Online Material

**Table 4.** Summary of our spectroscopic pulsation analysis of individual spectral lines in HD 24712. The columns give central wavelengths in Å, followed by the pulsation amplitude  $A$  (in  $\text{m s}^{-1}$ ), its error  $\sigma_A$  and the period  $P$  (in min) with the respective error estimate  $\sigma_P$  derived with a least-squares fit. Corresponding probability of periodic signal (Prob., calculated according to Home & Baliunas 1986). The next two groups of columns give pulsation amplitudes and phases  $\phi$  with the respective errors, determined with a simultaneous fit of two fixed pulsation periods indicated in the column head.

Wavelength Å	Free period					Fixed periods								Identification
	$A$ ( $\text{m s}^{-1}$ )	$\sigma_A$	$P$ (min)	$\sigma_P$	Prob.	$A$ ( $\text{m s}^{-1}$ )	$\sigma_A$	$\phi$	$\sigma_\phi$	$A$ ( $\text{m s}^{-1}$ )	$\sigma_A$	$\phi$	$\sigma_\phi$	
Hydrogen														
HARPS														
4340.468	59	15	6.237	0.041	0.847	22	18	0.132	0.132	44	18	0.759	0.067	H $\gamma$
4861.330	91	11	6.115	0.018	1.000	93	13	0.230	0.022	39	13	0.605	0.053	H $\beta$
6562.799	175	10	6.140	0.009	1.000	168	8	0.376	0.008	87	8	0.785	0.015	H $\alpha$
Na														
HARPS														
5895.996	37	12	3.831	0.018	0.368	30	14	0.581	0.077	20	14	0.656	0.118	Na I
Mg														
HARPS														
5172.701	22	6	3.862	0.017	0.644	20	7	0.656	0.062	14	7	0.759	0.088	Mg I
Si														
HARPS														
5701.115	113	40	5.501	0.043	0.122	35	50	0.209	0.069	43	49	0.343	0.025	Si I
5056.005	20	7	3.426	0.018	0.053	5	9	0.612	0.134	5	9	0.690	0.119	Si II
5978.939	82	23	4.418	0.022	0.700	89	28	0.558	0.051	66	28	0.707	0.069	Si II
6347.113	41	10	9.187	0.086	0.907	29	13	0.371	0.071	37	13	0.567	0.055	Si II
S														
HARPS														
4696.202	316	35	6.126	0.017	1.000	304	39	0.405	0.020	160	38	0.813	0.039	Si I + Nd III 4696.205
Ca														
HARPS														
4226.735	27	8	10.281	0.123	0.481	21	9	0.548	0.073	9	9	0.781	0.156	Ca I core
4425.444	16	5	6.207	0.049	0.388	11	6	0.356	0.087	11	6	0.849	0.091	Ca I
5349.471	25	7	3.302	0.014	0.616	13	9	0.246	0.117	5	9	0.428	0.119	Ca I
5590.124	34	13	3.065	0.016	0.376	2	16	0.535	0.147	14	15	0.759	0.020	Ca I
5857.467	30	9	8.749	0.094	0.503	21	11	0.313	0.087	24	11	0.622	0.075	Ca I
5867.564	147	36	5.794	0.033	0.925	141	45	0.227	0.051	47	45	0.403	0.152	Ca I bl.?
6122.224	28	7	6.149	0.040	0.825	26	9	0.211	0.055	14	9	0.632	0.098	Ca I
6162.198	34	10	4.562	0.024	0.574	18	12	0.506	0.106	12	12	0.129	0.156	Ca I
6163.760	63	22	4.329	0.026	0.149	18	27	0.311	0.076	42	27	0.138	0.102	Ca I
6439.107	30	7	6.175	0.038	0.926	24	8	0.470	0.057	18	8	0.921	0.076	Ca I
6462.592	21	6	6.221	0.046	0.568	8	7	0.105	0.147	15	7	0.665	0.080	Ca I
6471.673	56	13	6.082	0.035	0.941	59	16	0.346	0.043	30	16	0.692	0.085	Ca I
6493.793	48	12	6.116	0.038	0.896	54	14	0.825	0.044	18	15	0.128	0.125	Ca I
6499.655	26	8	10.094	0.132	0.303	19	10	0.978	0.090	5	10	0.420	0.155	Ca I
6717.705	53	55	3.060	0.027	0.005	26	19	0.227	0.118	46	19	0.354	0.067	Ca I
3933.655	126	21	6.134	0.025	0.999	121	25	0.816	0.033	43	25	0.243	0.093	Ca II core
5021.158	52	16	3.952	0.019	0.423	2	20	0.104	0.046	14	20	0.840	0.063	Ca II
5285.280	51	16	6.112	0.047	0.411	60	19	0.842	0.052	26	19	0.878	0.120	Ca II
Sc														
HARPS														
4415.579	143	12	6.135	0.013	1.000	130	14	0.366	0.017	55	14	0.829	0.041	Sc II + Nd III 4415.60
5239.807	251	17	6.135	0.010	1.000	251	14	0.396	0.009	139	14	0.781	0.016	Sc II + Ce II 5239.84
5526.831	53	11	6.027	0.031	0.986	54	13	0.397	0.040	35	13	0.708	0.063	Sc II + Ce II 5526.86
5641.007	516	358	3.049	0.006	0.354	84	75	0.340	0.141	87	74	0.313	0.139	Sc II
5657.908	80	20	9.500	0.092	0.854	26	26	0.267	0.001	37	26	0.423	0.116	Sc II + Fe II
Ti														
UVES1														
3444.295	114	14	6.113	0.020	1.000	111	18	0.229	0.026	35	18	0.494	0.081	Ti II + Dy II 3444.25
3491.039	58	9	6.096	0.028	0.999	63	12	0.065	0.032	23	12	0.384	0.083	Ti II
HARPS														
4518.038	96	32	5.122	0.035	0.237	55	40	0.055	0.116	4	40	0.666	0.075	Ti I
4913.636	108	33	3.427	0.014	0.493	15	41	0.865	0.098	35	41	0.680	0.026	Ti I
5016.182	117	36	3.934	0.018	0.462	78	44	0.511	0.091	50	45	0.522	0.141	Ti I
4422.380	25	8	3.679	0.018	0.223	21	10	0.039	0.077	3	10	0.294	0.045	Ti II
4464.470	29	5	6.061	0.025	0.999	32	6	0.990	0.030	12	6	0.273	0.075	Ti II
4501.267	94	6	6.118	0.010	1.000	98	4	0.436	0.008	53	4	0.799	0.014	Ti II + Nd III 4501.23
4529.513	13	5	7.566	0.082	0.095	10	6	0.002	0.096	3	6	0.467	0.121	Ti II
4563.774	30	3	6.177	0.018	1.000	24	3	0.066	0.025	19	3	0.514	0.032	Ti II
4583.409	90	24	6.083	0.039	0.820	81	29	0.387	0.056	17	28	0.910	0.102	Ti II
4708.683	37	13	9.331	0.119	0.086	28	15	0.797	0.088	9	15	0.415	0.102	Ti II
4805.105	35	8	6.149	0.033	0.976	31	9	0.225	0.048	14	9	0.693	0.107	Ti II
4911.212	27	8	8.466	0.085	0.581	33	9	0.957	0.046	19	9	0.167	0.077	Ti II
5005.194	63	19	7.388	0.067	0.449	30	23	0.275	0.124	44	23	0.801	0.086	Ti II
5013.706	56	13	8.238	0.061	0.974	35	16	0.181	0.074	16	16	0.471	0.005	Ti II
5129.176	22	6	3.418	0.013	0.845	20	7	0.131	0.057	14	7	0.301	0.085	Ti II
5185.918	19	3	6.127	0.028	0.998	20	4	0.977	0.033	12	4	0.338	0.057	Ti II
5226.562	17	4	6.160	0.036	0.937	13	4	0.097	0.058	7	4	0.647	0.111	Ti II
5418.794	58	12	8.912	0.066	0.992	28	16	0.359	0.091	34	16	0.590	0.074	Ti II
6491.602	70	23	8.052	0.085	0.162	51	29	0.951	0.090	30	29	0.056	0.152	Ti II





Table 4. continued.

Wavelength	Free period					Fixed periods								Identification
	A	$\sigma_A$	P	$\sigma_P$	Prob.	6.125 min				6.282 min				
	A	$\sigma_A$	$\phi$	$\sigma_\phi$		A	$\sigma_A$	$\phi$	$\sigma_\phi$	A	$\sigma_A$	$\phi$	$\sigma_\phi$	
3515.027 HARPS	70	10	6.145	0.026	1.000	65	14	0.385	0.033	30	13	0.622	0.074	Ni I
5035.398	80	29	4.155	0.024	0.042	38	35	0.215	0.145	40	35	0.582	0.138	Ni I
Sr														
UVES1														
3380.722	25	8	6.965	0.023	0.817	20	8	0.338	0.061	6	8	0.438	0.038	Sr II
3474.902	114	8	6.116	0.012	1.000	119	10	0.426	0.013	33	9	0.722	0.047	Sr II
HARPS														
4784.335	116	43	3.629	0.019	0.069	47	51	0.623	0.014	111	51	0.884	0.074	Sr I
4811.889	125	30	9.133	0.081	0.929	27	40	0.469	0.070	27	40	0.541	0.070	Sr I
4215.525	104	7	6.128	0.010	1.000	103	6	0.420	0.010	48	6	0.812	0.022	Sr II core
Y														
UVES1														
3549.001	71	9	6.133	0.022	0.999	74	10	0.722	0.023	49	10	0.024	0.035	Y II
HARPS														
5693.659	185	73	10.158	0.166	0.008	119	89	0.282	0.119	132	89	0.694	0.108	Y I
4883.686	82	9	6.092	0.016	1.000	89	10	0.728	0.018	43	10	0.060	0.037	Y II
4982.134	30	10	4.731	0.031	0.116	15	13	0.537	0.136	5	13	0.498	0.082	Y II
5087.427	51	5	6.129	0.016	1.000	52	5	0.693	0.018	27	5	0.075	0.034	Y II
5119.118	28	9	6.044	0.047	0.255	31	11	0.427	0.057	13	11	0.606	0.131	Y II
5289.824	65	19	3.312	0.012	0.626	34	24	0.917	0.110	9	23	0.748	0.072	Y II
5402.781	39	14	3.300	0.016	0.111	24	17	0.563	0.110	29	17	0.024	0.091	Y II
5509.901	30	7	6.049	0.037	0.885	34	9	0.533	0.043	18	9	0.741	0.082	Y II
5662.928	48	7	6.133	0.022	1.000	48	8	0.667	0.027	32	8	0.045	0.040	Y II
5728.899	45	16	3.576	0.018	0.073	20	20	0.360	0.155	17	20	0.539	0.022	Y II
6613.749	85	24	6.195	0.044	0.712	64	29	0.421	0.072	57	28	0.900	0.081	Y II bl.
Zr														
HARPS														
5350.379	168	24	6.189	0.022	1.000	114	29	0.340	0.041	89	29	0.873	0.053	Zr II?
Rh														
UVES1														
3434.865	64	18	3.196	0.014	0.603	18	26	0.420	0.067	22	25	0.679	0.022	Rh I
Pd														
UVES1														
3404.570	14	7	4.807	0.054	0.000	20	9	0.522	0.078	7	9	0.035	0.066	Pd I
HARPS														
5163.819	31	11	3.709	0.020	0.050	6	14	0.580	0.015	15	14	0.670	0.152	Pd I
5295.623	68	23	4.131	0.023	0.202	31	28	0.023	0.146	63	29	0.150	0.072	Pd I
In														
HARPS														
4511.263	254	31	6.173	0.011	1.000	228	36	0.351	0.025	177	36	0.756	0.033	In I
Ba														
HARPS														
4554.032	10	3	3.898	0.017	0.726	9	3	0.871	0.057	6	3	0.237	0.082	Ba II
4934.071	8	2	6.103	0.049	0.298	8	3	0.966	0.063	4	3	0.349	0.116	Ba II
5853.674	19	5	3.697	0.016	0.328	13	7	0.310	0.082	10	7	0.504	0.104	Ba II
6141.718	17	5	3.379	0.013	0.602	11	6	0.841	0.088	5	6	0.485	0.018	Ba II
6496.905	15	4	5.967	0.041	0.592	12	5	0.113	0.071	10	5	0.330	0.086	Ba II
La														
UVES1														
3517.010	88	5	6.110	0.011	1.000	98	6	0.475	0.010	42	6	0.802	0.024	La III
HARPS														
4526.097	113	9	6.160	0.013	1.000	97	10	0.385	0.017	52	10	0.851	0.032	La II
4574.857	113	12	6.164	0.017	1.000	99	13	0.384	0.022	66	13	0.820	0.033	La II
4655.474	155	16	6.118	0.015	1.000	152	17	0.328	0.019	74	17	0.728	0.038	La II
4662.504	151	15	6.108	0.015	1.000	160	14	0.432	0.015	102	14	0.786	0.023	La II
4692.489	107	19	6.119	0.026	0.999	107	23	0.301	0.034	1	23	0.563	0.127	La II
4740.261	170	12	6.140	0.011	1.000	160	11	0.426	0.011	91	11	0.841	0.020	La II
4748.724	134	16	6.162	0.019	1.000	120	18	0.401	0.025	77	18	0.831	0.039	La II
4804.026	123	20	6.095	0.024	0.999	129	23	0.360	0.029	57	23	0.710	0.065	La II
4921.802	146	12	6.133	0.013	1.000	137	12	0.486	0.015	72	12	0.907	0.028	La II
4986.837	82	11	6.141	0.020	1.000	83	11	0.394	0.023	56	11	0.767	0.034	La II
5482.256	128	33	6.078	0.038	0.880	118	40	0.241	0.055	16	40	0.782	0.066	La II
5797.557	93	15	6.103	0.025	0.999	89	18	0.391	0.032	52	17	0.790	0.055	La II
5805.766	159	30	6.087	0.028	0.998	164	36	0.364	0.035	45	36	0.703	0.125	La II
5808.295	144	32	6.101	0.033	0.973	158	38	0.179	0.039	36	38	0.234	0.011	La II
6262.283	183	32	6.150	0.026	0.999	145	38	0.292	0.042	91	37	0.815	0.067	La II + Pr II 6262.55
6296.074	161	30	6.152	0.028	0.999	141	36	0.313	0.041	42	35	0.861	0.137	La II
6320.376	84	13	6.136	0.023	1.000	79	14	0.293	0.030	44	14	0.710	0.053	La II
6399.017	133	42	4.142	0.022	0.339	114	52	0.376	0.073	50	52	0.595	0.005	La II
Ce														
UVES1														
3534.018	233	20	6.138	0.015	1.000	242	23	0.515	0.015	119	23	0.794	0.031	Ce II







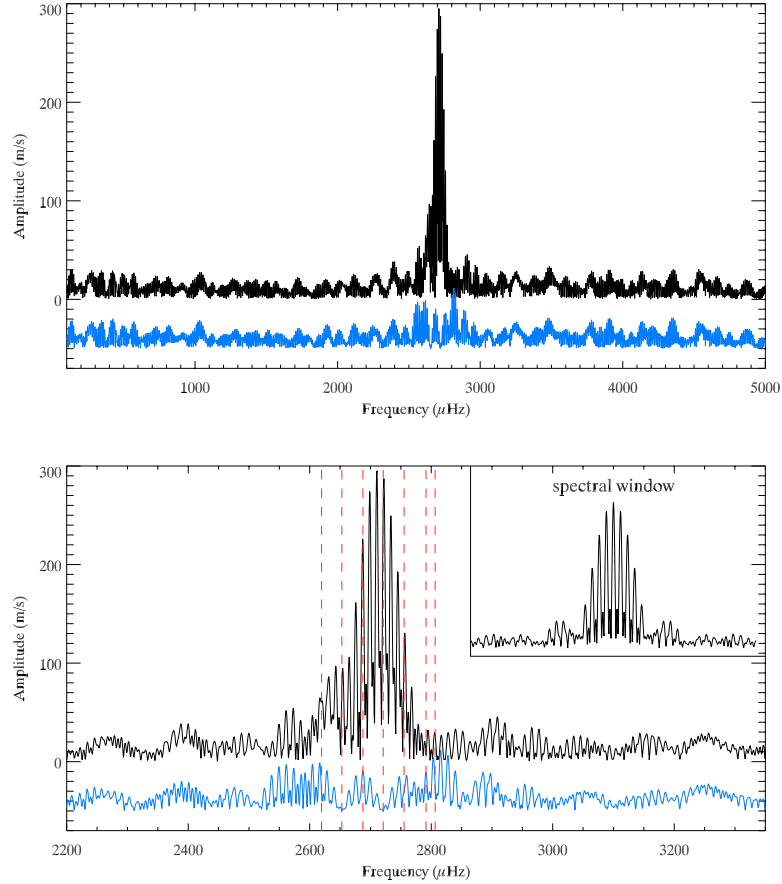






**Table 5.** Comparison of the pulsational amplitudes and phases near the magnetic maximum at different years calculated with the main pulsation period  $P = 6.125$  min in 2001 and 2004, and  $P = 6.20$  min in 2003.

WL Å	2001 phase = 0.872				2003 phase = 0.083				2004 phase = 0.867				2004 phase = 0.944				
	A	$\sigma_A$	$\phi$	$\sigma_\phi$	A	$\sigma_A$	$\phi$	$\sigma_\phi$	A	$\sigma_A$	$\phi$	$\sigma_\phi$	A	$\sigma_A$	$\phi$	$\sigma_\phi$	
5284.690					319	37	0.678	0.017	338	11	0.685	0.006	259	11	0.642	0.007	Pr III
5299.986					291	31	0.702	0.016	327	12	0.678	0.006	246	10	0.641	0.007	Pr III
5844.406					301	38	0.571	0.020	305	14	0.603	0.008	299	15	0.576	0.008	Pr III
5998.935					254	30	0.571	0.019	382	18	0.606	0.008	329	15	0.587	0.008	Pr III
6160.238					195	19	0.610	0.016	342	12	0.657	0.006	251	10	0.624	0.006	Pr III
6692.225	315	41	0.519	0.021					245	61	0.547	0.040	317	27	0.501	0.014	Pr III
6706.708	307	17	0.594	0.009	294	65	0.497	0.037	371	27	0.601	0.012	359	15	0.569	0.007	Pr III
4959.120					224	30	0.381	0.023	345	14	0.397	0.007	254	9	0.383	0.006	Nd II
5182.597					197	34	0.331	0.028	303	16	0.346	0.009	251	11	0.336	0.007	Nd II
5319.81					234	36	0.394	0.027					262	9	0.398	0.005	Nd II
6637.942	264	16	0.348	0.010					346	26	0.357	0.012	244	13	0.346	0.009	Nd II
6650.499	286	21	0.348	0.012					355	28	0.366	0.012	241	12	0.358	0.008	Nd II
6680.125					199	90	0.251	0.069	242	46	0.300	0.031	157	19	0.327	0.019	Nd II
5286.724					250	31	0.353	0.021	312	13	0.399	0.007	267	9	0.381	0.006	Nd III
5294.109					180	23	0.520	0.022	253	8	0.558	0.005	188	8	0.540	0.007	Nd III
5566.012					182	23	0.430	0.022	273	12	0.444	0.007	198	7	0.400	0.006	Nd III
5677.174					229	34	0.458	0.025	329	20	0.483	0.010	236	9	0.431	0.006	Nd III
5845.017					239	27	0.464	0.019	276	9	0.493	0.005	227	8	0.466	0.006	Nd III
5851.529					292	34	0.447	0.020	278	8	0.458	0.005	261	9	0.431	0.006	Nd III
5987.677					264	26	0.480	0.017	306	13	0.500	0.007	245	8	0.464	0.006	Nd III
6145.062					232	28	0.472	0.021	263	9	0.506	0.006	194	9	0.482	0.008	Nd III
6690.821	311	14	0.415	0.007	221	51	0.412	0.039	307	26	0.412	0.014	235	11	0.399	0.008	Nd III
6173.050					213	58	0.331	0.041	141	25	0.261	0.028	79	10	0.248	0.021	Eu II
6645.102	142	8	0.232	0.010					149	13	0.256	0.015	110	8	0.252	0.012	Eu II
5847.213					394	63	0.914	0.027	405	29	0.929	0.012	359	23	0.869	0.010	Tb III
6511.043					223	76	0.846	0.056	246	39	0.881	0.025	329	23	0.824	0.011	Tb III
6687.701	296	34	0.869	0.018					324	70	0.902	0.035	197	23	0.846	0.018	Tb III


**Fig. 9.** Amplitude spectra of Nd III spectral lines observed in 2001. In each panel the upper curve shows the original amplitude spectrum, whereas the lower curve (shifted downwards for better visibility) represents the Fourier transform of the RV-values after prewhitening with the two main RV frequencies of 2720.96 and 2652.96  $\mu\text{Hz}$ , which account for most of the RV power in the data set. The lower panel represents an enlarged view of the upper one. The spectral window of the data set is inserted. The vertical dashed lines indicate photometric frequencies according to Kurtz et al. (2005).